ISSN 1063-7745, Crystallography Reports, 2018, Vol. 63, No. 2, pp. 234–240. © Pleiades Publishing, Inc., 2018.
Original Russian Text © A.E. Muslimov, A.V. Butashin, V.M. Kanevsky, A.N. Deryabin, E.A. Vovk, V.A. Babaev, 2018, published in Kristallografiya, 2018, Vol. 63, No. 2, pp. 254–260.

SURFACE AND THIN FILMS

First Russian Crystallographic Congress

Manifestation of the Sapphire Crystal Structure in the Surface Nanopattern and Its Application in the Nitride Film Growth

A. E. Muslimov[a,*], A. V. Butashin[a], V. M. Kanevsky[a], A. N. Deryabin[a], E. A. Vovk[b], and V. A. Babaev[c]

[a] *Shubnikov Institute of Crystallography, Federal Scientific Research Centre "Crystallography and Photonics," Russian Academy of Sciences, Moscow, 119333 Russia*

[b] *Institute for Single Crystals, National Academy of Sciences of Ukraine, Kharkov, 61001 Ukraine*

[c] *Dagestan State University, Makhachkala, 367000 Russia*

**e-mail: amuslimov@mail.ru*

Received June 1, 2017

Abstract—The "quenching" technique was used to investigate the initial stage of the formation of a terrace-step nanostructure on the *R*-cut surface of sapphire crystal upon high-temperature annealing in air. The morphological features of the formation of *A*- and *R*-sapphire planes are experimentally shown in dependence on the misorientation direction and qualitatively interpreted with allowance for the surface energy density for the main sapphire faces. The possibilities of forming AlN layers on the *R*-sapphire surface with a terrace-step nanostructure under thermochemical effect and high-temperature substrate annealing in a mixture of nitrogen and reducing gases are considered.

DOI: 10.1134/S1063774518020141

INTRODUCTION

In view of the development of nanotechnologies, the interest of researchers in crystalline substrates with ordered surface nanorelief rapidly increases. These substrates are widely applied in various fields: epitaxial technologies [1, 2], deposition of supramolecular composites [3] and phthalocyanines [4], and formation of ordered nanocrystal arrays [5–9]. One of the main materials for crystalline substrates is sapphire due to its chemical and mechanical properties. Despite the existence of numerous studies [10–12] on the formation of terrace-step nanostructures (TSNs) on crystalline sapphire (α-Al_2O_3) substrates, there are no data on the initial stages of step nucleation and the dependence of their morphology on the misorientation direction and initial substrate surface roughness. On the whole, the data on the TSN formation for $A\{11\bar{2}0\}$-, $C\{0001\}$-, and $R\{10\bar{1}2\}$-cuts, obtained by different researchers, are often contradictory. In addition, the relationship between the TSN morphology for sapphire *A*-, *C*-, and *R*-cuts and the specific surface energy of faces, which is determined by their atomic structure, is sometimes disregarded. A simulation of the sapphire crystal surface energies and a comparison of the simulation results with experimental data were performed in [13, 14]. The following sequence of minimum surface energy values (normalized to area) was obtained:

$$C\{0001\} < R\{10\bar{1}2\} < A\{11\bar{2}0\} < M\{10\bar{1}0\}. \quad (1)$$

According to these results, the presence of faces with a lower specific surface energy may significantly hinder the formation of an ordered TSN, e.g., may lead to faceting [15]. Specific features of the TSN evolution on sapphire *C*-cuts were considered in detail in [16]. In this study, we investigate the processes of TSN formation and evolution on sapphire *R*- and *A*-cuts.

R-Cut sapphire substrates subjected to chemical mechanical polishing (CMP) are generally used in the silicon-on-sapphire epitaxy [17], because this cut has a fourfold pseudosymmetry. However, a preliminary thermal treatment of *R*-cut sapphire substrates with the formation of atomically smooth TSNs on their surface can be used as an important preliminary stage in epitaxy. The TSN height on the *R*-cut sapphire surface was estimated in [18] using layer-by-layer monitoring of the growth of aluminum oxide films by analyzing the intensity oscillations for diffracted electron reflections (high-energy electron diffraction (HEED)). The island height was found to be about 0.34 nm [18]; this value can be considered as the minimum TSN height for the *R*-cut. At the same time,

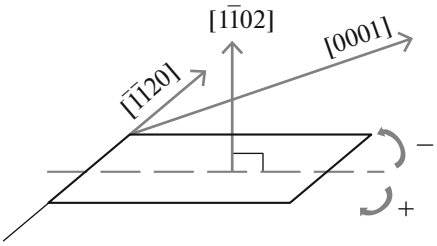

Fig. 1. Schematic diagram of directions for sapphire *R*-cut. Arrows and signs indicate possible *R*-cut misorientation via rotation around the [11$\bar{2}$0] axis in the negative or positive direction.

according to (1), ordered steps can be faceted by the C{0001} basal plane under certain conditions.

A-cut sapphire was successfully applied in [15] for the epitaxy of (111) indium oxide–tin (ITO) films. The minimum step height for the *A*-cut, calculated from structural data, was reported in [18, 19]; it is equal to the parameter $a/2$ of the sapphire structure (about 0.24 nm). In correspondence with (1), an ordered TSN formed on the *A*-cut can be faceted by the *C*{0001} and *R*{10$\bar{1}$2} planes.

We believe TSN-containing sapphire *C*- and *R*-cuts to be promising in the epitaxy of aluminum, gallium, and indium nitrides. One can obtain both polar and nonpolar AlN films based on these substrates. A technique of thermochemical nitridation at 1450°C was proposed in [20, 21] to grow AlN films. An application of this technique in nitridation of sapphire *C*-cuts was demonstrated in [22]; it was shown that heteroepitaxial ZnO films deposited on a nitrided surface of sapphire *C*-cut have a higher structural quality than those formed on sapphire. In this paper, we report the results of applying thermochemical nitridation of sapphire *R*-cuts to grow nonpolar AlN films.

EXPERIMENTAL

Sapphire *C*-, *R*-, and *A*-cuts subjected to CMP were used as substrates [23]. To form TSNs on the surface of substrates, the latter were annealed in air at temperatures of 1100–1400°C [11, 16]. The "quenching" technique [16] was used, which implies annealing of samples for 20–30 min with subsequent sharp cooling. Sapphire *R*-cuts were nitride at the Institute for Single Crystals, National Academy of Sciences of Ukraine, according to the technique described in [22]. The phase composition and orientation of crystallites in aluminum films after nitridation were determined using reflection HEED (electron diffractometer EMR 102, accelerating voltage 75 kV). The film surface morphology was investigated by atomic force microscopy (AFM) on an Ntegra Aura microscope (HT-MDT, Zelenograd) in the topography mode. Microscopic images of cuts were obtained by scanning electron microscopy (SEM) on a Helios electron microscope (FEI, United States) according to the conventional technique.

RESULTS AND DISCUSSION

Sapphire R-Cuts

To visualize the morphological transition from initial unformed steps to an atomically smooth structure, we chose sapphire *R*-cuts with a minimum step height of 0.34 nm. The misorientation direction was set (as in [24]) by negative rotation around the [11$\bar{2}$0] axis (Fig. 1) by an angle of 0.2°, because no faceting was observed by the authors at this misorientation.

The AFM surface images recorded in different recrystallization stages are shown in Fig. 2. The step height and terrace width in all stages was maintained at levels of 0.36 and 100 nm, respectively. To gain insight into the observed processes, it is necessary to take into account the transport mechanisms for individual atoms (molecules or aggregates), implemented both via diffusion over the surface and through the crystal bulk (according to the evaporation–condensation scheme). The former mechanism appears to be most likely for sapphire plates.

According to the AFM data (Fig. 2), pronounced diffusion processes in sapphire surface layers start being activated at temperatures above 1000°C, which is quite natural from the point of view of classical thermodynamics. The effect of reduced melting temperature in thin layers is well known [25–30]. The Tam-

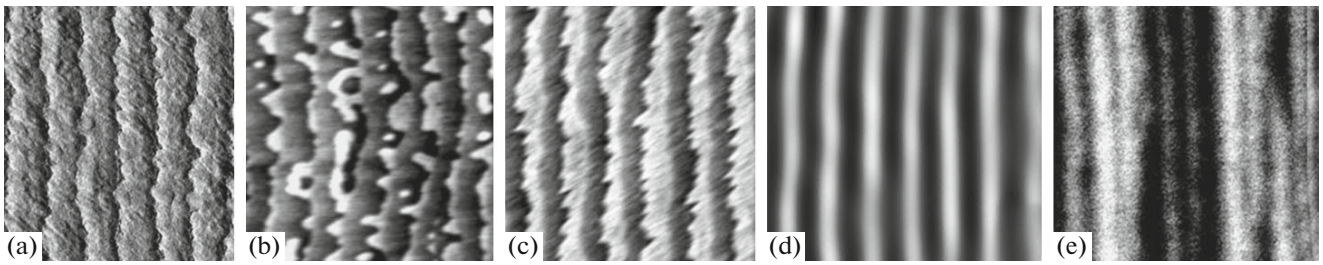

Fig. 2. AFM images of a TSN on a rhombohedral sapphire plane: (a) after CMP; (b, c) after 20-min annealing at 1050 and 1100°C, respectively; and (d, e) after 1-h annealing at 1100 and 1400°C, respectively; the image size is 700 × 700 nm^2.

mann temperature (T_T) is generally used to estimate roughly the onset of structural changes [31]:

$$T_T \approx 0.3–0.5T_0, \quad (2)$$

where $T_0 = 2040$°C is the sapphire melting temperature.

The vibrational spectrum of atoms on the crystal surface differs from the bulk spectrum. The vibrational amplitude of the surface atoms always exceeds that of the bulk ones. It was established that the Debye temperature T_D (at which all vibrational modes in solid become excited) of many metal and semiconductor single crystals decreases by half for the surface phase [32]. For sapphire, $T_D = 750–770$°C [33]; at temperatures below this value one might expect significant weakening of the elastic harmonic forces on the sapphire crystal surface.

Note that formula (2) does not take into account the case where the system is limited by a surface with energy comparable with the bulk energy. These conditions may reduce the melting temperature for the surface layers of crystal. Under these conditions the system tends to reduce its surface energy. This can be done by minimizing the surface area via melting. In this case, the melting temperature in the surface layers may be much lower than that of bulk crystal sapphire. With allowance for this possibility, formula (2) should take, according to [25], the following form:

$$T_{m-d} = T_0\left(1 - \frac{\sigma_s A_s}{\Delta HV} + \frac{\sigma_l A_l}{\Delta HV}\right), \quad (3)$$

where T_{m-d} is the temperature of solid–liquid phase transition; σ_s and σ_l are the surface energies; A_s and A_l are the surface areas of the solid and liquid phases, respectively, ΔH is the heat of fusion at the thin-film melting temperature T; and V is the volume of the system.

Since a crystal undergoes melting when its surface energy decreases to some value characteristic of this crystal [34], the following inequality holds true: $\sigma_s > \sigma_l$. A dependence of T_{m-d} on the decrease in the surface area of the system at the phase transition also follows from (3). Being polished, the crystal surface becomes inhomogeneous: a deeper layer of higher structural quality is coated by a looser damaged layer up to few angstroms thick. This structure can be presented as a loose aluminum oxide layer coating a sapphire substrate. The surface area of the loose layer multiply exceeds the corresponding area of atomically smooth crystal surface. Therefore, the $\sigma_s A_s$ value may be many times larger than $\sigma_l A_l$. In correspondence with (3), this should lead to a significant decrease in the melting temperature for sapphire surface layers of angstrom thickness with a minimum volume V. However, melting regions have not been observed on sapphire surface upon high-temperature (above 1000°C) annealing in diffraction studies. Nevertheless, according to the AFM data (Fig. 2b), a two-dimensional "liquid-like" phase arises. Presumably, heating a loose sapphire surface layer to 1050°C leads to the formation of "liquid-like" regions; the driving force of this order–disorder transition is the tendency of the system to lowering the surface energy. Pronounced "submelting" starts with the loosest regions (exterior angles of edges) and propagates towards the interior step angles. On the assumption that there is a loose homoepitaxial aluminum oxide layer on the sapphire surface, the substrate is not inert; therefore, dispersion into individual clusters does not occur. The total surface energy of the system decreases due to the growth of "liquid-like" phase, which shifts equilibrium between the "liquid-like" and solid phases to higher temperatures. Such a large amount of material cannot exist in the liquid-like phase at this temperature; therefore, simultaneous crystallization starts easily (because no energy should be spent on the interface formation) (Fig. 2b) [35]. Heating at 1050°C for 1 h would lead to the final formation of an atomically smooth crystal structure, which was observed by other researchers. In the case under consideration, the process was "frozen" due to the sharp cooling of the system, and the "liquid-like" phase underwent solidification in the potential crystal field (Fig. 2b). This pattern is confirmed by the AFM data on the sapphire surface annealed at a higher temperature: 1100°C (Fig. 2c). In this stage, crystallization is almost complete, with formation of atomically smooth steps having diffuse boundaries. When visualizing steps by the phase contrast method, one can see that the recrystallization occurs (Fig. 3) from the reentrant angle towards the step plateau edge.

Upon further annealing at 1100°C and higher temperatures, after the step formation, the key role is played by diffusion flows along the surface, which exponentially increase with temperature in correspondence with the Arrhenius formula

$$D_S \sim \exp(-E_A/kT), \quad (4)$$

where E_A is the surface diffusion activation energy (energy-barrier height). As can be seen in Fig. 2d, the atoms diffusing along the surface tend to rectify a step, i.e., reduce its length and kink density. Annealing at 1400°C does not lead to further coarsening of steps (Fig. 2e); on the contrary, it deteriorates their morphology. At high temperatures sapphire surface may also degrade (Fig. 4a), with conservation of step height at a level of about 0.36 nm.

In the case of R-cut misorientation along the $[11\bar{2}0]$ direction, a TSN may be faceted by the basal plane, which, according to [13, 14], has the least specific surface energy. We chose supersmoothly polished samples of R-cuts misoriented up to 0.5° with respect to the $[11\bar{2}0]$ direction. A study of the annealing of these plates at a temperature above 1200°C demonstrated the formation of a nanorelief faceted by the basal plane (Fig. 4b). This specific feature of R-cuts

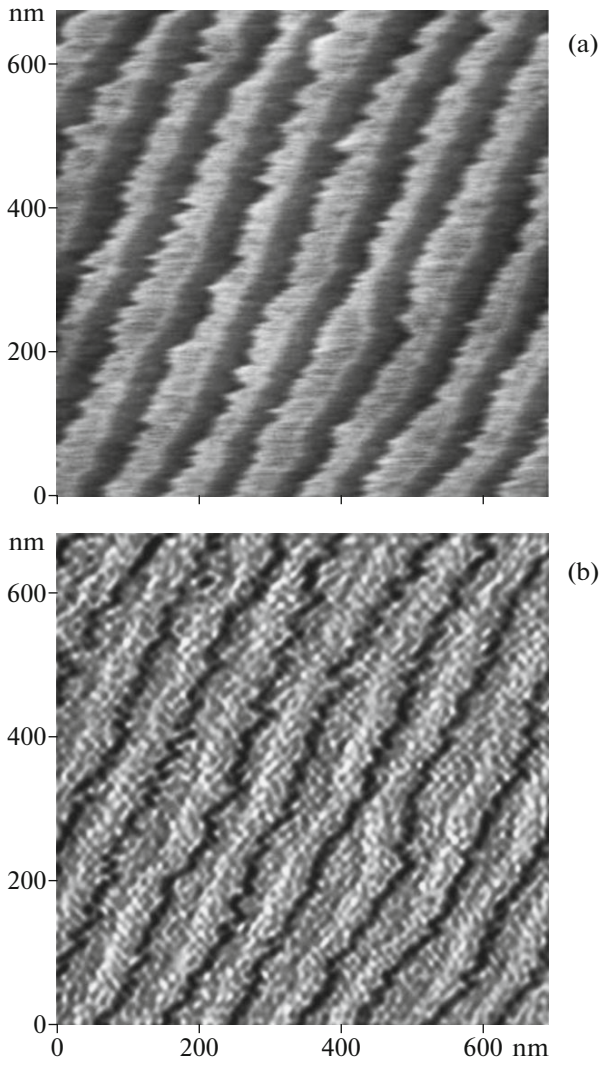

Fig. 3. AFM images of a TSN on a sapphire *R*-cut after CMP and annealing (1100°C, 20 min): (a) topography and (b) phase contrast.

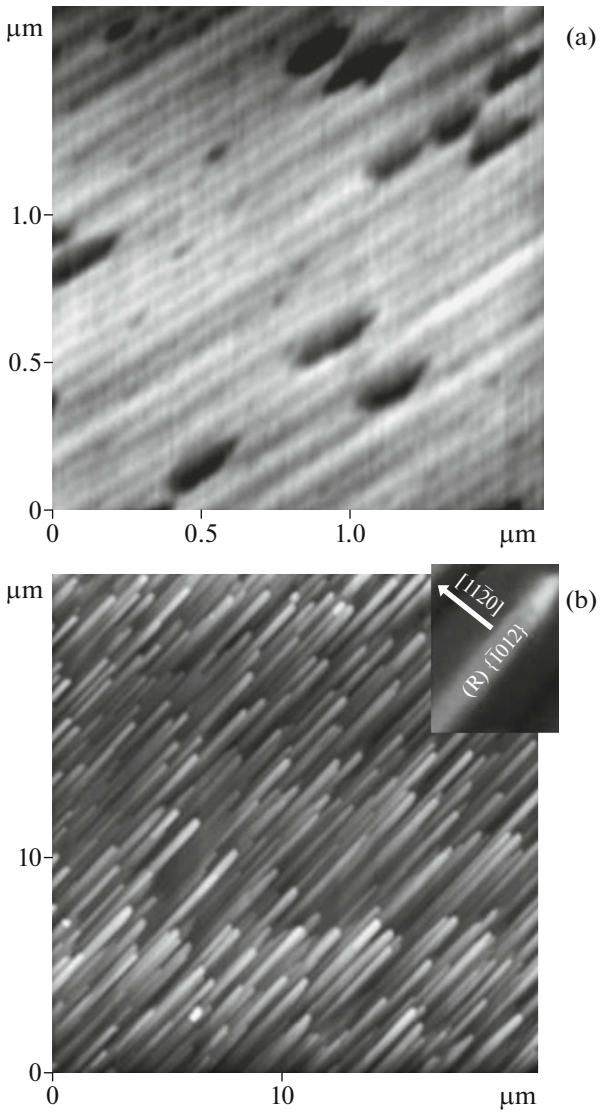

Fig. 4. (a) AFM image of a sapphire *R*-cut with a TSN misoriented in the negative direction around the [11$\bar{2}$0] axis (Fig. 1) after annealing at 1400°C. (b) AFM image of the sapphire *R*-cut along the [11$\bar{2}$0] direction after annealing at 1200°C. The inset shows a fragment of an individual step.

must be taken into account when choosing plates for epitaxy.

Sapphire A-Cuts

When TSNs are formed on sapphire *A*-cuts, in correspondence with (1), there may be a problem of their faceting by sapphire *R*- and *C*-planes due to their lower surface energy. Most likely, one can obtain an ordered TSN with pronounced directionality by setting misorientation with respect to the [0001] direction (Fig. 5).

We prepared sapphire *A*-cut plates with roughnesses of about 0.2 and 0.3 nm and identical misorientation with respect to the *C*-plane direction (about 0.2°) for experiments (Fig. 6). Steps become pronounced at a temperature of 1100°C; their height is 0.25 nm, a value close to the half lattice parameter $a/2$ [18, 19] of the sapphire structure. As can be seen in Fig. 6, the step height does not increase during annealing to 1400°C. However, the TSN morphology depends strongly on the initial roughness of sapphire plates subjected to CMP (Figs. 6a, 6b). With an increase in roughness, TSNs acquire a hillock-like structure.

The morphology of TSNs formed on sapphire *A*-cut plates changes significantly at random misorientation with preferred deviation of the normal to the *A* plane towards the *M*-plane direction (Fig. 6c).

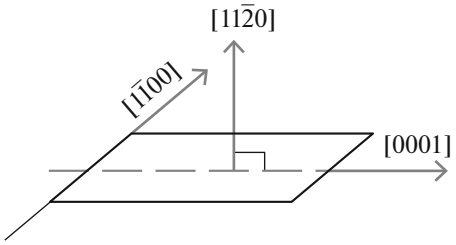

Fig. 5. Schematic diagram of directions for sapphire *A*-cut.

The surface acquires a faceted microrelief at 1200°C; the corresponding TSN (Fig. 6c) is an intermittent structure of steps faceted by *A* and *M* planes, which is crossed by faces with *C* and *R* orientations.

Formation of AlN Films on Sapphire R-Cuts with TSNs

The surface state of *R*-cut sapphire plates radically changes with a change in the high-temperature annealing atmosphere; i.e., when air is replaced with a mixture of nitrogen and reducing gases. According to the AFM (Fig. 7a), SEM (Fig. 7b), HEED (Fig. 7a, inset), and X-ray diffraction data, a continuous single-crystal AlN film with a hexagonal wurtzite-type structure is formed on an *R*-sapphire substrate after thermochemical nitridation. Indexing of diffraction data shows that the nonpolar (11$\bar{2}$0) face of the AlN film is oriented parallel to the (10$\bar{1}$2) plane of the sapphire substrate. No additional reflections (due to domains and twins) are observed in this case. Electron microscopy reveals a clear interface between the AlN film with a thickness of about 300 nm and the substrate (Fig. 7b). The film has a mosaic structure: one can observe individual single-crystal AlN blocks with lateral sizes of 100–200 nm. The film mosaicity is also evidenced by some broadening of diffraction reflections in the electron diffraction pattern (Fig. 7a). It is also noteworthy that block boundaries coincide with steps on the sapphire surface (Fig. 7b). Single-crystal AlN blocks in the film are associated with individual atomically smooth terraces on the sapphire surface. Most likely, TSNs play a key role in the surface nitridation: since diffusion is facilitated on step edges, they serve as formation sites for new phase nuclei. Note that the TSN observed on the sapphire substrate surface (Fig. 7b) was formed during its thermochemical nitridation as a result of etching in reducing medium at high temperature (1450°C) [36].

An AlN film nucleates on the *R*-sapphire face during thermochemical nitridation of Al_2O_3 on the surface according to the reaction [20]

$$Al_2O_3(s) + 3CO(g) + N_2(g) = 2AlN(s) + 3CO_2(g), \quad (5)$$

and the rate of further growth of AlN film is limited by the rates of nitrogen diffusion to the AlN–Al_2O_3 interface and oxygen diffusion to the AlN–gas medium interface.

The epitaxial relationship $(11\bar{2}0)\langle 1\bar{1}00\rangle AlN \parallel (10\bar{1}2)\langle 1\bar{2}10\rangle Al_2O_3$ (Fig. 8) is due to the positional similarity of the sites of both lattices in the (11$\bar{2}$0) AlN and (10$\bar{1}$2) Al_2O_3 planes. Sites of both lattices have an almost square arrangement with a lattice parameter of 0.5 nm. The parameter mismatch for these rectangles is much smaller than the mismatch between the AlN and Al_2O_3 lattices for other versions of mutual orientation of lattices in epitaxial growth of these crystals [20]. We should also take into account that, according to

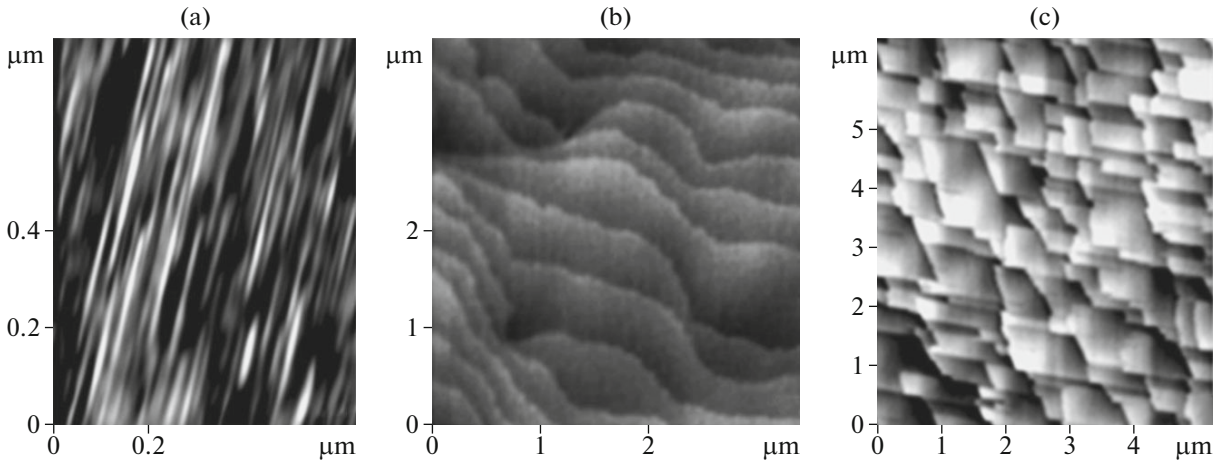

Fig. 6. (a, b) AFM images of a TSN on a sapphire *A*-cut misoriented with respect to the *C*-plane direction, after CMP and annealing at 1400°C; the initial plate roughness is about (a) 0.2 and (b) 0.3 nm. (c) AFM image of a randomly misoriented sapphire *A*-cut after annealing at 1200°C.

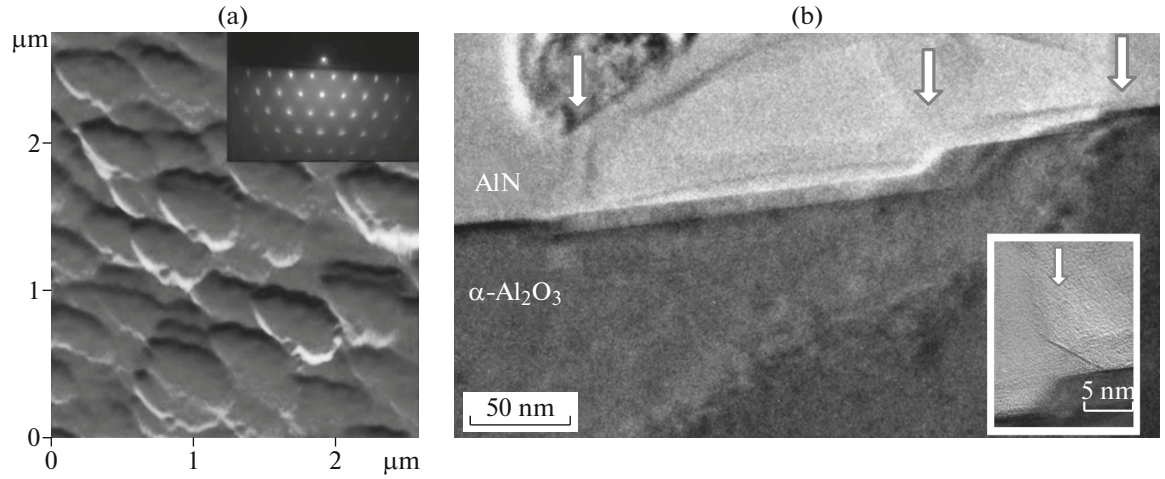

Fig. 7. (a) Two-dimensional AFM image of the surface and (b) an SEM image of the interface for the film $(11\bar{2}0)$ AlN ∥ $(10\bar{1}2)$ Al_2O_3. The insets show (a) an HEED pattern of this film and (b) an arbitrary area of the film interface on enlarged scale. Arrows indicate block boundaries.

reaction (5), AlN is formed from Al_2O_3 by exchanging anions with the gas medium, whereas cations remain in the solid phase. Based on this consideration, one can suggest that, starting with the nucleation onset, the crystalline AlN film is strictly oriented with respect to the *R* plane of Al_2O_3 crystal. Despite the fact that a model of AlN film formation during solid-phase transformations at thermochemical nitridation of sapphire surface was reported in [20], the study in this field should be continued.

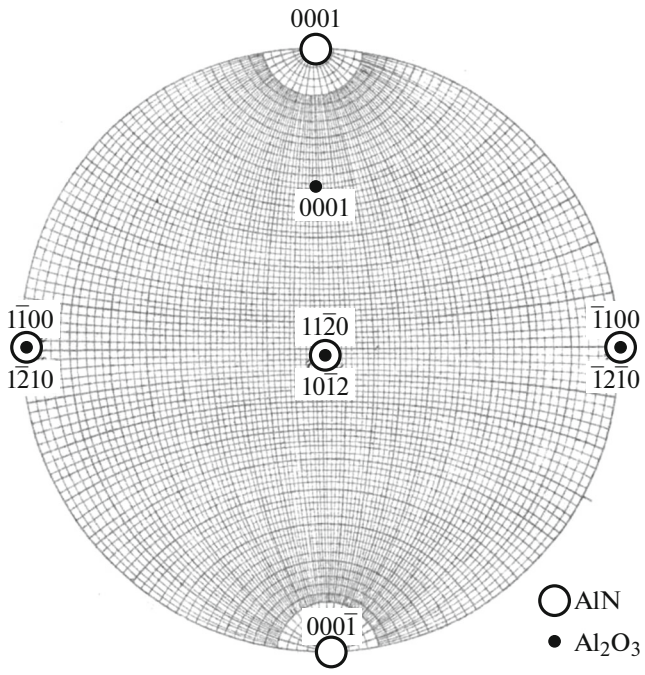

Fig. 8. Gnomostereographic projection of AlN film on $(10\bar{1}2)$ Al_2O_3.

CONCLUSIONS

The quenching technique and AFM were used to investigate the initial stage of TSN formation on the sapphire *R*-cut surface. A mechanism taking into account the decrease in the melting temperature for a loose material layer with a high specific surface energy and the formation of a liquid-like precipitate was proposed. An ordered TSN with steps of 0.36 nm in height, which do not grow upon heating to a temperature of 1400°C, was found to be formed on sapphire *R*-cuts misoriented by an angle of 0.2° with respect to the $[11\bar{2}0]$ axis (negative rotation in Fig. 1). A nanorelief faceted by the basal plane is formed on the sapphire *R*-cut misoriented with respect to the $[11\bar{2}0]$ direction and annealed at a temperature above 1200°C. A TSN with a step height of 0.25 nm is formed on *A*-cut plates misoriented with respect to the *C*-plane direction by an angle of 0.2° after annealing at a temperature of 1100°C; the steps of this TSN do not grow during annealing to 1400°C. The TSN morphology depends strongly on the initial plate roughness after the CMP stage; the TSN acquires a hillock-like structure with an increase in roughness. In the case of random misorientation of *A*-cut sapphire plates with preferred deviation of the normal to the *A* plate towards the *M*-plane direction, the surface acquires a faceted microrelief at 1200°C. The observed specific features of TSNs and their high-temperature evolution on different cuts were qualitatively interpreted taking into account the data on the surface energy density for the main sapphire faces. These features for sapphire *A*- and *R*-cuts must be taken into account when choosing plates for epitaxy. SEM was used to investigate the interface for AlN films of nonpolar $(11\bar{2}0)$ orientation, formed by thermochemical nitridation on sapphire substrates with an ordered TSN.

ACKNOWLEDGMENTS

The study was performed using the equipment of the Mixed-Use Center of the Shubnikov Institute of Crystallography, Federal Scientific Research Centre "Crystallography and Photonics," Russian Academy of Sciences, and supported by the Ministry of Education and Science of the Russian Federation; the Federal Agency of Scientific Organizations (agreement no. 007-ГЗ/Ч3363/26); and the Russian Foundation for Basic Research, project no. 16-29-11763 ofi-m (in the part concerning the structural study of epitaxial aluminum nitride films on sapphire substrates).

REFERENCES

1. V. I. Mikhailov, A. V. Butashin, V. M. Kanevskii, et al., Poverkhnost, No. 6, 97 (2011).
2. A. V. Butashin, V. M. Kanevskii, A. E. Muslimov, et al., Crystallogr. Rep. **59** (3), 418 (2014).
3. J. Kao, S.-J. Jeong, Z. Jiang, et al., Adv. Mater. **26**, 2777 (2014).
4. E. Barrena, J. O. Ossó, F. Schreiber, et al., J. Mater. Res. **19**, 2061 (2004).
5. A. Ismach, D. Kantorovich, and E. Joselevich, J. Am. Chem. Soc. **127**, 11554 (2005).
6. F. Cuccureddu, V. Usov, S. Murphy, et al., Rev. Sci. Instrum. **79** (5), 053907 (2008).
7. J. Y. Son, S. J. Lim, J. H. Cho, et al., Appl. Phys. Lett. **93**, 053109 (2008).
8. A. E. Muslimov, A. V. Butashin, A. A. Konovko, et al., Crystallogr. Rep. **57** (3), 415 (2012).
9. A. E. Muslimov, A. V. Butashin, B. V. Nabatov, et al., Crystallogr. Rep. **62** (2), 300 (2017).
10. Y. Shiratsuchi, M. Yamamoto, and Y. Kamada, Jpn. J. Appl. Phys. **41**, 5719 (2002).
11. A. V. Butashin, V. P. Vlasov, V. M. Kanevskii, et al., Kristallografiya **57** (5), 927 (2012).
12. K. Maruyama, M. Yoshikawa, and H. Takigawa, J. Cryst. Growth **93**, 761 (1988).
13. S. I. Bakholdin and V. N. Maslov, Phys. Solid State **57** (6), 1236 (2015).
14. Yu. G. Nosov, S. I. Bakholdin, and V. M. Krymov, Tech. Phys. **54** (2), 239 (2009).
15. S. Curiotto and D. Chatain, Surf. Sci. **603**, 2688 (2009).
16. V. P. Vlasov, A. E. Muslimov, A. V. Butashin, and V. M. Kanevskii, Crystallogr. Rep. **61** (1), 58 (2016).
17. H. M. Manasevit and W. I. Simpson, J. Appl. Phys. **35**, 1349 (1964).
18. T. Maeda, M. Yoshimoto, T. Ohnishi, et al., J. Cryst. Growth **177**, 95 (1997).
19. M. Y. Chern, Y. C. Huang, and W. L. Xu, Thin Solid Films **515** (20–21), 7866 (2007).
20. Kh. Sh.-O. Kaltaev, N. S. Sidel'nikova, S. Nizhankovskii, et al., Semiconductors **43** (12), 1606 (2009).
21. H. Fukuyama, Sh. Kusunoki, A. Hakomori, and K. Hiraga, J. Appl. Phys. **100**, 024905 (2006).
22. A. V. Butashin, V. M. Kanevskii, A. E. Muslimov, et al., Crystallogr. Rep. **60** (4), 565 (2015).
23. I. A. Prokhorov, B. G. Zakharov, B. S. Roshchin, et al., Crystallogr. Rep. **56** (3), 456 (2011).
24. M. Araki, N. Mochimizo, K. Hoshino, and K. Tadatomo, Jpn. J. Appl. Phys. **47** (1), 119 (2008).
25. D. G. Gromov, S. A. Gavrilov, and E. N. Redichev, Zh. Fiz. Khim. **79** (9), 1578 (2005).
26. D. G. Gromov, S. A. Gavrilov, E. N. Redichev, and R. M. Ammosov, Phys. Solid State **49** (1), 178 (2007).
27. S. S. Belousov, S. A. Gavrilov, D. G. Gromov, et al., Izv. Vyssh. Uchebn. Zaved., Elektron., No. 1, 15 (2007).
28. L. J. Lewis, P. Jensen, and J.-L. Barrat, Phys. Rev. B **56**, 2248 (1997).
29. R. Kofman, P. Cheyssac, Y. Lereah, and A. Stella, Eur. Phys. J. D **9**, 441 (1999).
30. F. Celestini, R. J.-M. Pellenq, P. Bordarier, and B. Rousseau, Phys. D **37**, 9 (1996).
31. M. A. Korzhuev, Fiz. Khim. Obrab. Mater., No. 5, 153 (1993).
32. V. F. Kiselev, S. N. Kozlov, and A. V. Zoteev, *Fundamentals of Solid Surface Physics* (Izd-vo MGU, Moscow, 1999) [in Russian].
33. M. V. Klassen-Neklyudova, Kh. S. Bagdasarov, P. M. Belyaev, et al., *Ruby and Sapphire* (Nauka, Moscow, 1974) [in Russian].
34. M. N. Magomedov, Phys. Solid State **46** (5), 954 (2004).
35. D. G. Gromov and S. A. Gavrilov, Phys. Solid State **51** (10), 2135 (2009).
36. S. I. Krivonogov, A. A. Krukhmalev, S. V. Nizhankovskii, et al., Crystallogr. Rep. **60** (1), 138 (2015).

Translated by Yu. Sin'kov